Acta Cryst. (1998). A**54**, 416–429

Symmetrical X-ray Diffraction in a Perfect Rectangular $t \times l$ Crystal. Extinction and Absorption

GUNNAR THORKILDSEN* AND HELGE B. LARSEN

Department of Mathematics and Natural Science, Stavanger College, Ullandhaug, 4004 Stavanger, Norway.
E-mail: gunnar.thorkildsen@tn.his.no

(*Received 19 November 1997; accepted 24 December 1997*)

Abstract

The boundary-value Green function technique has been used with the Takagi–Taupin equations to explore analytically the diffraction in a perfect rectangular $t \times l$ crystal for a symmetrical coplanar scattering mode. The important contribution is the development of the integration structure over the entrance and exit surfaces of the crystal. A single parameter, $\zeta = (t/l)\tan\theta_{oh}$, maps the different crystals and the scattering geometries. In the limits $\zeta \to 0$ and $\zeta \to \infty$, the well known functions for the primary extinction factors for perfect semi-infinite crystals in the case of Laue and Bragg scattering are retrieved. Numerical integrations extend the range of applicability of the method. Both ordinary absorption and generalized extinction, *i.e.* the joint effect on the kinematical integrated power due to multiple scattering and resonant scattering, are addressed. Germanium is used as a model system for some of the calculations.

1. Introduction

One of the main problems in dealing with dynamical diffraction in perfect crystals is to take the finite crystal shape into consideration. Approaches based on the fundamental theory, *cf.* Zachariasen (1945) or Pinsker (1978), are in principle only valid for crystals having an infinite laterally extended diffraction plane. In a previous paper (Thorkildsen & Larsen, 1998), hereafter denoted TL, we have shown that the Takagi–Taupin equations (Takagi, 1962, 1969; Taupin, 1964) combined with the boundary-value Green function technique comprise a powerful tool to analytically handle the calculations of dynamical scattering in perfect spherical and cylindrical crystals.

In this paper, we use the same concepts to analyse dynamical scattering in a perfect crystal with a rectangular-shaped diffraction plane. Uragami (1969, 1970, 1971), in his work on *Pendellösung* fringes in finite crystals, introduces the division of the crystal into regions and gives closed expressions for the diffracted fields for both Laue and Bragg scattering. His results are used for numerical calculations in this work. Saka *et al.* (1972*a*,*b*, 1973), *cf.* Kato (Azároff *et al.*, 1974), analysed and classified the wave fields for different geometrical conditions in polyhedral crystals. Later, Olekhnovich & Olekhnovich (1978) used the ideas of Uragami to numerically calculate the primary extinction factor in a square-cross-section parallelepiped crystal for a limited range of the Bragg angle. Becker (1977) and Becker & Dunstetter (1984) made important contributions advocating the *point-source* formalism and the concept of *an extended volume* to handle scattering in finite crystals. A renewed interest in the problem is due to the development of Bragg–Fresnel zone plates (Snigirev & Suvorov, 1993) in which rectangular edges and surface profiling of silicon single crystals have been used for the focusing of a periodic object.

In the present work, we treat the case of symmetrical coplanar scattering. The main development is a general integration structure for the entrance and exit surfaces which makes it possible to handle any $t \times l$ cross section. The general theoretical foundations are given in §2. In §3, we apply the formalism to calculate extinction and absorption factors. Both a symbolic calculation based on a series-expansion approach and a

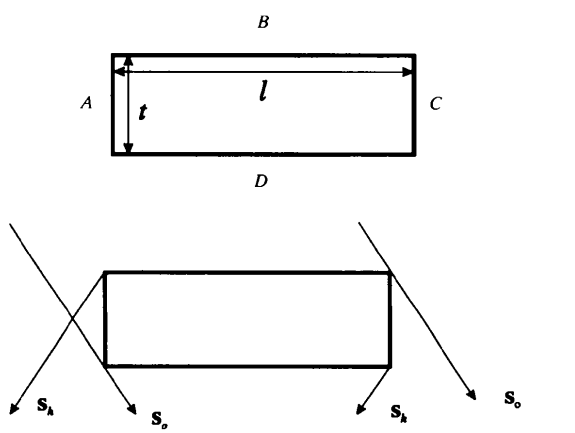

Fig. 1. Crystal dimensions and face labels. Entrance surfaces are *A* and *B*, exit surfaces *A* and *D*. The angle between $\mathbf{s}_o$ and $\mathbf{s}_h$ is $2\theta_{oh}$.

numerical calculation using Uragami's results are performed.

2. Theory

2.1. *General*

We seek the integrated diffracted power, $\mathcal{P}_h$, from a perfect $t \times l$ crystal when it is subject to an incoming *plane wave* with wave vector in the direction of $\mathbf{s}_o$. The direction of the diffracted wave is $\mathbf{s}_h$. Fig. 1 shows the actual geometry.

In TL, it was shown that the integrated diffracted power can be expressed by

$$\mathcal{P}_h = \mathcal{P}_h^{(0)}(1/v \sin 2\theta_{oh}) \sum_r \sum_{m=m'(r)} \int dz \int_{M(m)} \mathbf{s}_h \cdot d\mathbf{M} \times \int_{S(M)} \mathbf{s}_o \cdot d\mathbf{S} |G_h(\Delta_o, \Delta_h | m; r)|^2 \times \exp[-\mu(\Delta_o + \Delta_h)]. \quad (1)$$

$\mathcal{P}_h^{(0)}$ is the kinematical integrated power. v is the volume of the crystal and θ_{oh} is the Bragg angle. The set of functions $\{i\kappa_{ho} G_h\}$ are the boundary-value Green functions for the wave field† $\tilde{D}_h$. They are the solutions of the Takagi–Taupin equations for two beams written in the representation

$$\partial \tilde{D}_o / \partial s_o = i\kappa_{oh} \tilde{D}_h \quad (2)$$

$$\partial \tilde{D}_h / \partial s_h = i\kappa_{ho} \tilde{D}_o \quad (3)$$

with the boundary condition

$$\tilde{D}_o(S) = \delta(s_h). \quad (4)$$

S is a source point on the entrance surface and δ denotes Dirac's δ function.

Separate functions G_h exist in each region m, which are bounded by the characteristic lines associated with the equations, *cf.* Sommerfeld (1949) and Sneddon (1957). These regions originate as a consequence of the limits imposed on the wave propagation by the crystal boundaries. It is usual to differentiate between a Laue ($r = \mathsf{L}$) and a Bragg ($r = \mathsf{B}$) family of regions, depending on the position of S on the entrance surface, *cf.* §2.2. The coordinates (Δ_o, Δ_h) represent the differences $[s_o(M) - s_o(S), s_h(M) - s_h(S)]$, where M is a point on the exit surface. Fig. 2 shows two point sources, with associated local coordinate systems, located on the A and B parts of the entrance surface, respectively. A global coordinate system, (r_0, r_1), which will serve as a reference for the surface integrations, is also shown. The relations that exist between the various coordinate systems are explored in Appendix A.

† Consult TL Section 2.1 for a rigorous definition of the field functions $\tilde{D}_o$ and $\tilde{D}_h$.

It is convenient to treat the diffracted field at the exit as a superposition of four discrete scattering processes depending on the possible combinations of the positions of S and M on the crystal surfaces. We denote the processes as A–A, A–D, B–A and B–D scattering, *cf.* Fig. 1. The integration $\int_{S(M)} \mathbf{s}_o \cdot d\mathbf{S}$ sums up the contributions from all sources S which give rise to a diffracted wave at the exit point M. In the same way, the integration $\int_{M(m)} \mathbf{s}_h \cdot d\mathbf{M}$ sums the contributions from all exit points. The integration limits depend upon a geometrical factor, ζ, which is defined in §2.2. Each region m, at the exit, is treated separately. The vectors $\mathbf{s}_o$ and $\mathbf{s}_h$ define a diffraction plane at a height z along the vertical extension of the crystal. m' is the subset of regions that contributes at the exit.

In equation (1), μ is the linear absorption coefficient, thus the effect of absorption along the optical routes caused by the multiple-scattering events is included in the calculations. Furthermore, as will become evident, the functions G_h will depend upon the product of structure factors, $F_h F_{-h}$, since†

$$\kappa_{ho}\kappa_{oh} = (r_e \lambda C / V_c)^2 F_h F_{-h}. \quad (5)$$

In the general case when resonant scattering is included, this parameter will become a complex quantity:

$$\kappa_{ho}\kappa_{oh} = |\kappa_{ho}\kappa_{oh}| \exp(i\Phi) \quad (6)$$

$$\Phi = \varphi_{oh} + \varphi_{ho}. \quad (7)$$

φ_{pq} is the single phase associated with κ_{pq}. In this work, we define the *extinction length* by

$$\Lambda_{oh} \stackrel{\text{def}}{=} 1/(|\kappa_{ho}\kappa_{oh}|)^{1/2}. \quad (8)$$

Owing to the variation of the anomalous scattering functions f' and f'' with the wavelength, we will have $F_h = F_h(\lambda)$ and $\Phi = \Phi(\lambda)$.

† All symbols have their standard interpretation: r_e: classical electron radius, λ: wavelength, C: polarization factor, V_c: unit-cell volume, F_h: structure factor.

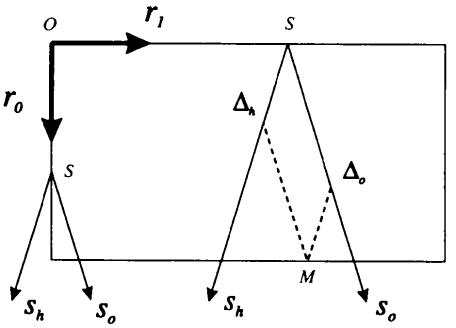

Fig. 2. Actual coordinate systems used.

2.2. *Region structure*

The region structure associated with a source point on the A surface is shown in Fig. 3. The corresponding region structure with source point on B is shown in Fig. 4. The number of regions present at the exit is linked to the value of the parameter ζ defined by:

$$\zeta = (t/l)\tan\theta_{oh}. \tag{9}$$

This parameter thus comprises both the crystal dimension, (t, l), and the scattering condition, θ_{oh}. Figs. 5 and 6 indicate the build up of contributions with increasing value of ζ. Depending on the position of the source point, different regions are realised at a given exit point and we have to add the field amplitudes. This is sorted out through the integration set-up, *cf.* §2.5. For a pyramidal or bipyramidal shaped crystal, we have that $\zeta = \zeta(z)$.

It should be noted that the topology of the region structures presented here is identical to that of a crystal with a circular diffraction plane, *cf.* TL.

2.3. *Calculation procedure*

To simplify the implementation in the mathematical software system *Mathematica*,† the analysis will be carried out using dimensionless coordinates. All lengths‡ are scaled to the characteristic length ℓ defined by

$$\ell = (l/2\sin\theta_{oh}). \tag{10}$$

In general, $\ell = \ell(z)$ but here we will only consider parallelepiped shaped crystals, *i.e.* crystals with a fixed cross section in the vertical direction.

The Takagi–Taupin equations become:

$$\partial\tilde{D}_o/\partial s_o = i\kappa_{oh}\ell\tilde{D}_h \tag{11}$$

$$\partial\tilde{D}_h/\partial s_h = i\kappa_{ho}\ell\tilde{D}_o \tag{12}$$

and we express the integrated power by the equation†

$$\mathcal{P}_h = \mathcal{P}_h^{(0)}(1/2\zeta)\sum_{\mathsf{S}}\sum_{m=m'(\zeta;\mathsf{S})}\int_{M(\zeta;m,\mathsf{S})}\mathrm{d}y\int_{S(y,\zeta;m,\mathsf{S})}\mathrm{d}x \times |G_h(\Delta_o, \Delta_h|m; r_{\mathsf{S}})|^2\exp[-\mu_0(\Delta_o + \Delta_h)]. \tag{13}$$

S counts the actual surface combinations (A–A, A–D, B–A, B–D). Furthermore, we have $r_{A-A} = r_{A-D} = \mathsf{B}$ and $r_{B-A} = r_{B-D} = \mathsf{L}$, labelling the Bragg and Laue families of Green functions. The expressions for Δ_o and Δ_h, using the new variables x and y, are given in Table

† *Mathematica* is a trademark of Wolfram Research Inc., Champaign, IL 61820, USA.

‡ Including parameters a and b introduced in Figs. 3 and 4.

† The relations between the x and y coordinates and the positions of source and exit points measured in (r_0, r_1) are given in Appendix A.

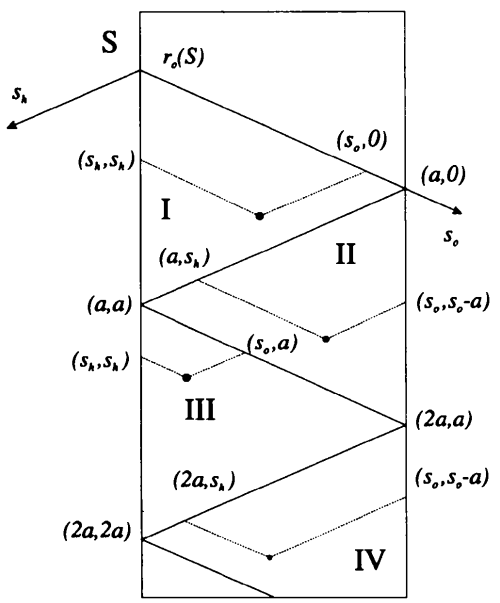

Fig. 3. The Bragg family of regions, or regions with source S on the A surface. • represent points (s_o, s_h) within the crystal. $a = l/\sin\theta_{oh}$.

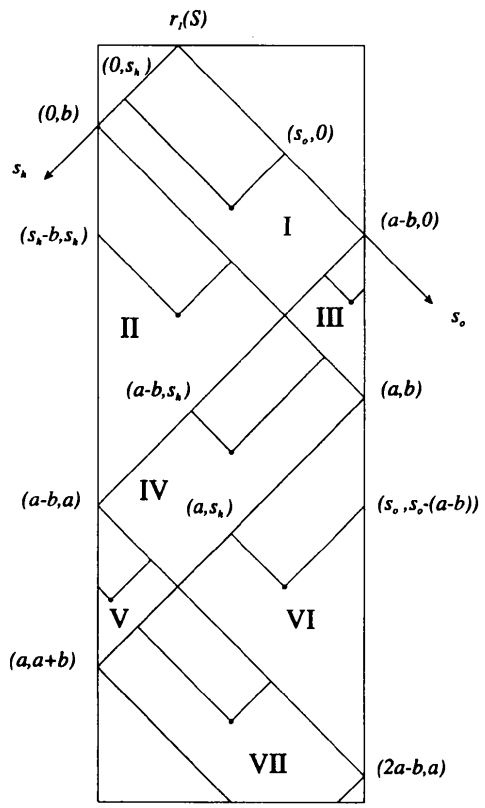

Fig. 4. The Laue family of regions, or regions with source S on the surface B. $a = l/\sin\theta_{oh}$ and $b = r_1(S)/\sin\theta_{oh}$.

1. In this table, we have also included the actual expressions for $c \stackrel{\text{def}}{=} b/\ell$. The definitions of x and y are chosen to simplify the mathematical treatment, especially the surface integrations and the implementation in *Mathematica*.

μ_0, a dimensionless absorption coefficient, is defined by:

$$\mu_0 \stackrel{\text{def}}{=} \mu\ell. \tag{14}$$

To obtain analytical expressions or numerical values for $\mathcal{P}_h$, we have to find:

(*a*) the families of functions: $G_h(s_o, s_h|m; r)$;

(*b*) the surface integration set-up: $\int_{M(\zeta;m,S)} dy \int_{S(y,\zeta;m,S)} dx$.

2.4. *Field solutions*

The extinction factor is usually expressed as a series expansion in the squared ratio of characteristic length to extinction length. This leads us to express the boundary-value Green functions as series and search for the expansion coefficients. Such an approach will be outlined in the first part of this section. The results are suitable for symbolically calculating the various terms in a series for the generalized extinction factor for a perfect crystal. Physically, the terms in the series represent multiple scattering–rescattering events. In the second part, it is pointed out that the series for G_h can be given in closed forms. Here we directly apply the results of Uragami (1969, 1970, 1971) adopted to the notation used in this paper. These functions are suitable for numerical integrations.

Table 1. *Coordinates Δ_o and Δ_h for an exit point M relative to a source point S, expressed in dimensionless coordinates x and y with $c = b/\ell$*

S	Δ_o	Δ_h	c
A–A	x	x	–
A–D	$x+2y$	x	–
B–A	$2y-x$	x	$2x-2y$
B–D	$2\zeta-x$	x	$2x+2y-2\zeta$

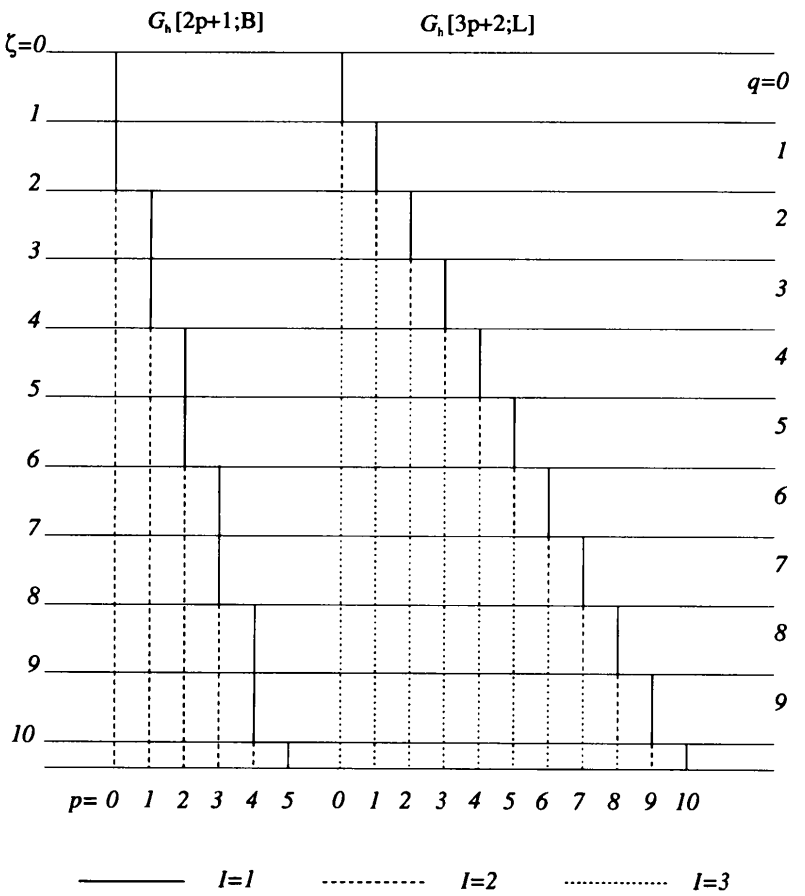

Fig. 5. Contributions to the field at the exit surface *A*.

2.4.1. *Series expansions for the family of Green functions.* The boundary-value Green functions are formally expressed by the series:

$$\tilde{D}_o(s_o, s_h) = (1/\ell) \sum_{n=0}^{\infty} (-u)^n G_o^{(n)}(s_o, s_h) \tag{15}$$

$$\tilde{D}_h(s_o, s_h) = i\kappa_{ho} G_h(s_o, s_h) = i\kappa_{ho} \sum_{n=0}^{\infty} (-u)^n G_h^{(n)}(s_o, s_h), \tag{16}$$

where the expansion parameter u is given by

$$u = \kappa_{oh}\kappa_{ho}\ell^2. \tag{17}$$

Using equations (11) and (12), we obtain the recurrence relations

$$\partial G_o^{(n)}(s_o, s_h)/\partial s_o = G_h^{(n-1)}(s_o, s_h) \qquad n \geq 1 \tag{18}$$

$$\partial G_h^{(n)}(s_o, s_h)/\partial s_h = G_o^{(n)}(s_o, s_h) \qquad n \geq 1 \tag{19}$$

together with

$$\partial G_o^{(0)}(s_o, s_h)/\partial s_o = 0$$

$$\partial G_h^{(0)}(s_o, s_h)/\partial s_h = G_o^{(0)}(s_o, s_h).$$

Applying the boundary condition associated with the point source, equation (4), we find the following conditions for those sections of the crystal where first-order scattering is present:

$$G_o^{(0)}(s_o, s_h) = \delta(s_h) \tag{20}$$

$$G_h^{(0)}(s_o, s_h) = \Theta(s_h). \tag{21}$$

Θ denotes the Heaviside function. We then obtain the integral recurrence relations and boundary conditions, from which it becomes possible to calculate the series-expansion coefficients:

$$\begin{aligned} G_o^{(n)}(s_o, s_h|m; r) &= G_o^{(n)}(s_o^b, s_h|m^b; r) + \int_{s_o^b}^{s_o} \mathrm{d}s'_o \, G_h^{(n-1)}(s'_o, s_h|m; r) \\ &= G_o^{(n)}(s_o^b, s_h|m^b; r) + \mathcal{L}_{oh}^{(m;r)} G_h^{(n-1)}(s'_o, s_h|m; r) \end{aligned} \tag{22}$$

$$\begin{aligned} G_h^{(n)}(s_o, s_h|m; r) &= G_h^{(n)}(s_o, s_h^b|m^b; r) + \int_{s_h^b}^{s_h} \mathrm{d}s'_h \, G_o^{(n)}(s_o, s'_h|m; r) \\ &= G_h^{(n)}(s_o, s_h^b|m^b; r) + \mathcal{L}_{ho}^{(m;r)} G_o^{(n)}(s_o, s'_h|m; r). \end{aligned} \tag{23}$$

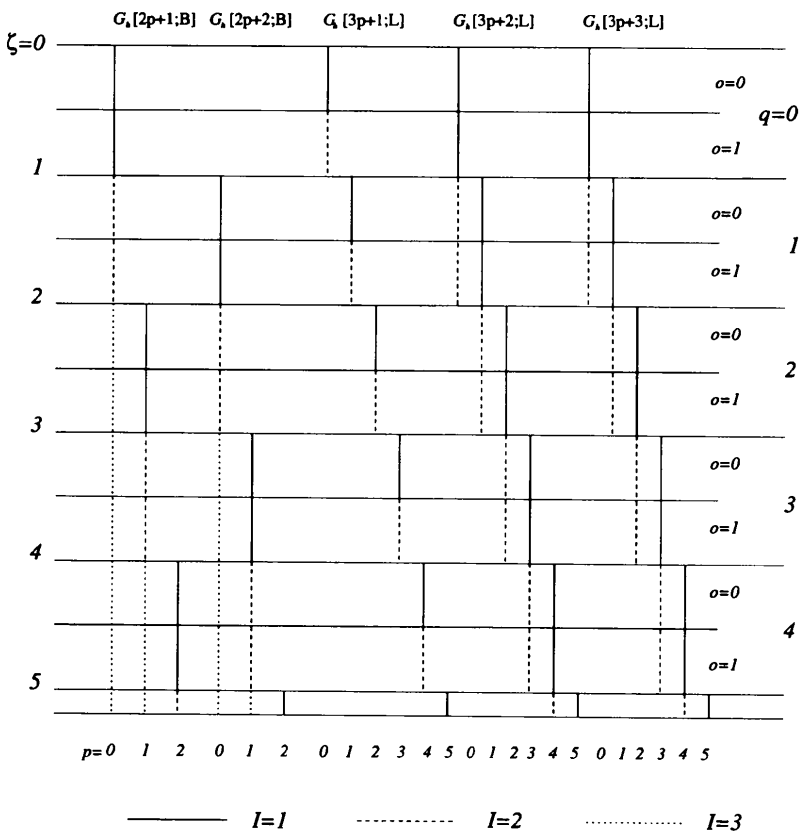

Fig. 6. Contributions to the field at the exit surface D.

$G_o^{(0)}(s_o, s_h|m; r) = 0$ at a general interior point ($s_h \neq 0$)

$G_h^{(0)}(s_o, s_h^b|m^b; r) = 0$ on the rear surface C (no diffracted wave emitted)

$G_h^{(0)}(s_o, s_h|1; \mathsf{B}) = 1$

$G_h^{(0)}(s_o, s_h|m; \mathsf{B}) = 0 \quad m \geq 2$

$G_h^{(0)}(s_o, s_h|1; \mathsf{L}) = 1$

$G_h^{(0)}(s_o, s_h|2; \mathsf{L}) = 1$

$G_h^{(0)}(s_o, s_h|m; \mathsf{L}) = 0 \quad m \geq 3.$

The boundary conditions correspond to those used by Uragami (1971). s_o^b and s_h^b are coordinates for the boundary points for the region in question. m^b represents a neighbouring region or the crystal boundary. In general, the functions $G_o^{(n)}$ and $G_h^{(n)}$ are continuous across a region border for any order n. The integral operators $\mathcal{L}_{ho}$ and $\mathcal{L}_{oh}$, implicitly defined in equations (22) and (23), are given in Tables 2 and 3.

By applying the recurrence relations, equations (22) and (23), it is possible to analytically calculate the coefficients $G_h^{(n)}(s_o, s_h|m; r)$ in principle to any order n.

2.4.2. *Closed expressions for the fields.* Using the work of Uragami (1971), we find recurrence relations for the boundary-value Green functions expressed in closed forms. The results are:†

Laue family:

$$G_h(s_o, s_h|3p+1; \mathsf{L}) = G_h(s_o, s_h|3p-2; \mathsf{L}) + w(s_o, s_h|3p-1; \mathsf{L}) + w(s_o, s_h|3p; \mathsf{L}) \quad (24)$$

$$G_h(s_o, s_h|3p+2; \mathsf{L}) = G_h(s_o, s_h|3p+1; \mathsf{L}) + w(s_o, s_h|3p+2; \mathsf{L}) \quad (25)$$

$$G_h(s_o, s_h|3p+3; \mathsf{L}) = G_h(s_o, s_h|3p+1; \mathsf{L}) + w(s_o, s_h|3p+3; \mathsf{L}); \quad (26)$$

Bragg family:

$$G_h(s_o, s_h|2p+1; \mathsf{B}) = G_h(s_o, s_h|2p; \mathsf{B}) + w(s_o, s_h|2p+1; \mathsf{B}) \quad (27)$$

$$G_h(s_o, s_h|2p+2; \mathsf{B}) = G_h(s_o, s_h|2p+1; \mathsf{B}) + w(s_o, s_h|2p+2; \mathsf{B}); \quad (28)$$

where we have

$$G_h(s_o, s_h|1; \mathsf{L}) = J_0\left[2(us_os_h)^{1/2}\right] \quad (29)$$

$$G_h(s_o, s_h|1; \mathsf{B}) = J_0\left[2(us_os_h)^{1/2}\right] + (s_h/s_o)J_2\left[2(us_os_h)^{1/2}\right]. \quad (30)$$

In the Laue case, it is convenient to handle regions with p even and p odd separately. Thus, the region counters

† J_n is the Bessel function of order n.

Table 2. *Defining integral operators for the Bragg family, $r = \mathsf{B}$; $p = 0, 1, \ldots$*

Region	$\mathcal{L}_{oh}^{(m;\mathsf{B})}$	$\mathcal{L}_{ho}^{(m;\mathsf{B})}$
$m = 2p+1$	$\int_{s_h}^{s_o} \mathrm{d}s_o'$	$\int_{2p}^{s_h} \mathrm{d}s_h'$
$m = 2p+2$	$\int_{2(p+1)}^{s_o} \mathrm{d}s_o'$	$\int_{s_o-2}^{s_h} \mathrm{d}s_h'$

Table 3. *Defining integral operators for the Laue family, $r = \mathsf{L}$; $p = 0, 1, \ldots$ and $c = b/\ell$*

Region	p	$\mathcal{L}_{oh}^{(m;\mathsf{L})}$	$\mathcal{L}_{ho}^{(m;\mathsf{L})}$
$m = 3p+1$	Odd	$\int_{(p+1)-c}^{s_o} \mathrm{d}s_o'$	$\int_{(p-1)+c}^{s_h} \mathrm{d}s_h'$
	Even	$\int_{p}^{s_o} \mathrm{d}s_o'$	$\int_{p}^{s_h} \mathrm{d}s_h'$
$m = 3p+2$	Odd	$\int_{s_h-c}^{s_o} \mathrm{d}s_o'$	$\int_{p+1}^{s_h} \mathrm{d}s_h'$
	Even	$\int_{s_h-c}^{s_o} \mathrm{d}s_o'$	$\int_{p+c}^{s_h} \mathrm{d}s_h'$
$m = 3p+3$	Odd	$\int_{p+1}^{s_o} \mathrm{d}s_o'$	$\int_{s_o-(2-c)}^{s_h} \mathrm{d}s_h'$
	Even	$\int_{(p+2)-c}^{s_o} \mathrm{d}s_o'$	$\int_{s_o-(2-c)}^{s_h} \mathrm{d}s_h'$

will be of the type $6p + i$ with $p = 0, 1, \ldots$ and $i = 1, \ldots, 6$. The actual functions $w(s_o, s_h|m; \mathsf{L})$ then become:

$$w(s_o, s_h|6p+2; \mathsf{L}) = (-1)^p\{[s_h - (2p+c)]/[s_o + (2p+c)]\}^{p+1} \times J_{2p+2}\left(2\{u[s_o + (2p+c)][s_h - (2p+c)]\}^{1/2}\right) \quad (31)$$

$$w(s_o, s_h|6p+3; \mathsf{L}) = (-1)^{p+1}\left(\{s_o - [(2p+2) - c]\} \times \{s_h + [(2p+2) - c]\}^{-1}\right)^p \times J_{2p}\left[2\left(u\{s_o - [(2p+2) - c]\} \times \{s_h + [(2p+2) - c]\}\right)^{1/2}\right] \quad (32)$$

$$w(s_o, s_h|6p+5; \mathsf{L}) = (-1)^{p+1}\{[s_h - (2p+2)]/[s_o + (2p+2)]\}^{p+1} \times J_{2p+2}\left(2\{u[s_o + (2p+2)][s_h - (2p+2)]\}^{1/2}\right) \quad (33)$$

$$w(s_o, s_h|6p+6; \mathsf{L}) = (-1)^{p+1}\{[s_o - (2p+2)]/[s_h + (2p+2)]\}^{p+1} \times J_{2p+2}\left(2\{u[s_o - (2p+2)][s_h + (2p+2)]\}^{1/2}\right). \quad (34)$$

In the Bragg case, we have:

$$w(s_o, s_h|2p+1; \mathsf{B}) = (-1)^p[(s_h - 2p)/(s_o + 2p)]^{p+1} \times J_{2p+2}\{2[u(s_o + 2p)(s_h - 2p)]^{1/2}\} + (-1)^p[(s_h - 2p)/(s_o + 2p)]^p \times J_{2p}\{2[u(s_o + 2p)(s_h - 2p)]^{1/2}\} \quad (35)$$

Table 4. *Relations between exit and entrance surface integration; A–A scattering*

m	ζ	I	y	x
$2p+1$	$(2p, 2p+2)$	1	$(2p, \zeta)$	$(2p, y)$
	$(2p+2, \infty)$	2*a*	$(2p, 2p+2)$	$(2p, y)$
		2*b*	$(2p+2, \zeta)$	$(2p, 2p+2)$

Table 5. *Relations between exit and entrance surface integration; A–D scattering*

m	ζ	I	y	x
$2p+1$	$(2p, 2p+1)$	1	$(0, \zeta-2p)$	$(2p, \zeta-y)$
	$(2p+1, 2p+2)$	2*a*	$(0, 2p+2-\zeta)$	$(2p, \zeta-y)$
		2*b*	$(2p+2-\zeta, 1)$	$(2p, 2p+2-2y)$
	$(2p+2, \infty)$	3	$(0, 1)$	$(2p, 2p+2-2y)$
$2p+2$	$(2p+1, 2p+2)$	1	$(2p+2-\zeta, 1)$	$(2p+2-2y, \zeta-y)$
	$(2p+2, 2p+3)$	2*a*	$(0, \zeta-2p-2)$	$(2p+2-2y, 2p+2)$
		2*b*	$(\zeta-2p-2, 1)$	$(2p+2-2y, \zeta-y)$
	$(2p+3, \infty)$	3	$(0, 1)$	$(2p+2-2y, 2p+2)$

Table 6. *Relations between exit and entrance surface integration; B–A scattering*

m	ζ	I	y	x
$3p+2$	$(p, p+1)$	1	(p, ζ)	$(p+1, y+1)$
p odd	$(p+1, p+2)$	2*a*	$(p, p+1)$	$(p+1, y+1)$
		2*b*	$(p+1, \zeta)$	$(2y-p-1, y+1)$
	$(p+2, \infty)$	3*a*	$(p, p+1)$	$(p+1, y+1)$
		3*b*	$(p+1, p+2)$	$(2y-p-1, y+1)$
$3p+2$	$(p, p+1)$	1	(p, ζ)	$(y, 2y-p)$
p even	$(p+1, p+2)$	2a	$(p, p+1)$	$(y, 2y-p)$
		2*b*	$(p+1, \zeta)$	$(y, p+2)$
	$(p+2, \infty)$	3*a*	$(p, p+1)$	$(y, 2y-p)$
		3*b*	$(p+1, p+2)$	$(y, p+2)$

$$
\begin{aligned}
&w(s_o, s_h|2p+2; \mathsf{B}) \\
&\quad = (-1)^{p+1}\{[s_o - (2p+2)]/[s_h + (2p+2)]\}^{p+1} \\
&\qquad \times J_{2p+2}\big(2\{u[s_o - (2p+2)][s_h + (2p+2)]\}^{1/2}\big) \\
&\qquad + (-1)^{p+1}\{[s_o - (2p+2)]/[s_h + (2p+2)]\}^{p} \\
&\qquad \times J_{2p}\big(2\{u[s_o - (2p+2)][s_h + (2p+2)]\}^{1/2}\big). \qquad (36)
\end{aligned}
$$

2.5. *Surface integrations*

The set-up for the surface integrations is summarized in Tables 4 to 7. The parameter I is used as a reference for a given integration. It is introduced to simplify the reading of the tables in conjunction with Figs. 5 and 6, which show the contributions to the diffracted field at the exit surfaces. The $G_h(s_o, s_h|m = m'; r)$ functions are not defined outside the limits in ζ given in the tables. *I.e.* the regions m' are only realised at the exit for specific values of the parameter ζ. The integration set-up depends on the value of ζ or, explicitly, the related integer (Int[ ]) values q and o, defined by

$$q = \text{Int}[\zeta] \qquad (37)$$

$$o = \text{Int}[2 \times (\zeta - q)]. \qquad (38)$$

The subdivision of the integer intervals (q) in ζ, designated by o $(o = 0 \vee 1)$, naturally appears from the analysis that gives the integration structure for the *B–D* scattering terms, *cf.* §3.1.

Independent of the values of q and o, the surface integrations should give the result

$$\sum_{\mathsf{S}} \sum_{m=m'(\zeta;\mathsf{S})} \int_{M(\zeta;m,\mathsf{S})} \mathrm{d}y \int_{S(y,\zeta;m,\mathsf{S})} \mathrm{d}x = 2\zeta[1 + (\zeta/4)]. \quad (39)$$

This follows from the analysis given by Becker (1977), who showed that the surface integrations always can be transformed to a 'volume' integration for an extended volume v', *cf.* Fig. 7.

2.6. *Generalized extinction factor and absorption factor*

Having the series expansion for G_h, we can construct

$$|G_h(\Delta_o, \Delta_h|m; r_{\mathsf{S}})|^2 = \sum_{n=0}^{\infty}(-1)^n|u|^n I_h^{(n)}(\Delta_o, \Delta_h; \Phi|m; r_{\mathsf{S}}) \qquad (40)$$

with

$$
\begin{aligned}
&I_h^{(n)}(\Delta_o, \Delta_h; \Phi|m; r_{\mathsf{S}}) \\
&\quad = \sum_{k=0}^{n} G_h^{(k)}(\Delta_o, \Delta_h|m; r_{\mathsf{S}}) G_h^{(n-k)}(\Delta_o, \Delta_h|m; r_{\mathsf{S}}) \\
&\qquad \times \exp[i(2k - n)\Phi].
\end{aligned}
$$

By construction, the coefficients $\{G_h^{(k)}\}$ are real functions.

It is found convenient† to express the generalized extinction factor, y, for the perfect $t \times l$ crystal formally by

$$
\begin{aligned}
y = (\mathcal{P}_h/\mathcal{P}_h^{(0)}) &= y(\zeta, \mu_0, \Phi, \xi) \\
&= \sum_{n=0}^{\infty}(-1)^n f_n^{(q)}(\zeta, \mu_0, \Phi)\xi^n \qquad (41)
\end{aligned}
$$

† We have here already adopted one of the results from the analysis. The coefficients $f_n^{(q)}$ do not depend on the parameter o. In general, the number of parameters included in the definition of $f_n^{(q)}$ will depend on the actual problem that is considered.

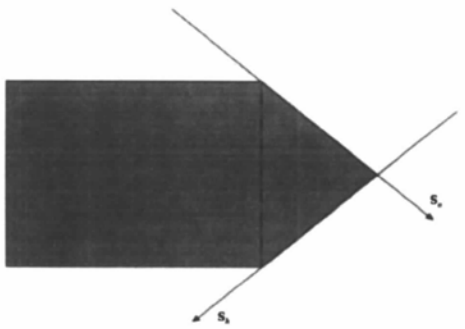

Fig. 7. Extended volume v' for a crystal in the shape of a rectangular parallelepiped. $v' = 2\zeta(1 + \zeta/w)l^2 \sin 2\theta_{oh}$.

Table 7. *Relations between exit and entrance surface integration; B–D scattering*

m	ζ	I	y	x
$3p+1$	$(p, p+\frac{1}{2})$	1*a*	$(0, \zeta-p)$	$(p+1-2y, p+1)$
p odd		1*b*	$(\zeta-p, p+1-\zeta)$	$(p+1-2y, 2\zeta-2y-p+1)$
		1*c*	$(p+1-\zeta, 1)$	$(2\zeta-p-1, 2\zeta-2y-p+1)$
	$(p+\frac{1}{2}, p+1)$	2*a*	$(0, p+1-\zeta)$	$(p+1-2y, p+1)$
		2*b*	$(p+1-\zeta, \zeta-p)$	$(2\zeta-p-1, p+1)$
		2*c*	$(\zeta-p, 1)$	$(2\zeta-p-1, 2\zeta-2y-p+1)$
$3p+1$	$(p, p+\frac{1}{2})$	1*a*	$(0, \zeta-p)$	$(2\zeta-2y-p, 2\zeta-p)$
p even		1*b*	$(\zeta-p, p+1-\zeta)$	$(p, 2\zeta-p)$
		1*c*	$(p+1-\zeta, 1)$	$(p, p+2-2y)$
	$(p+\frac{1}{2}, p+1)$	2*a*	$(0, p+1-\zeta)$	$(2\zeta-2y-p, 2\zeta-p)$
		2*b*	$(p+1-\zeta, \zeta-p)$	$(2\zeta-2y-p, p+2-2y)$
		2*c*	$(\zeta-p, 1)$	$(p, p+2-2y)$
$3p+2$	$(p, p+1)$	1	$(0, \zeta-p)$	$(p+1, \zeta-y+1)$
p odd	$(p+1, p+2)$	2	$(0, p+2-\zeta)$	$(2\zeta-p-1, \zeta-y+1)$
$3p+2$	$(p, p+1)$	1	$(0, \zeta-p)$	$(\zeta-y, 2\zeta-2y-p)$
p even	$(p+1, p+2)$	2	$(0, p+2-\zeta)$	$(\zeta-y, p+2-2y)$
$3p+3$	$(p, p+1)$	1	$(p+1-\zeta, 1)$	$(\zeta-y, 2\zeta-p-1)$
p odd	$(p+1, p+2)$	2	$(\zeta-p-1, 1)$	$(\zeta-y, p+1)$
$3p+3$	$(p, p+1)$	1	$(p+1-\zeta, 1)$	$(p+2-2y, \zeta-y+1)$
p even	$(p+1, p+2)$	2	$(\zeta-p-1, 1)$	$(2\zeta-2y-p, \zeta-y+1)$

with expansion coefficient

$$f_n^{(q)}(\zeta, \mu_0, \Phi) = (1/2\zeta^{(2n+1)}) \sum_{\mathsf{S}} \sum_{m=m_n'(\zeta;\mathsf{S})} \int_{M(\zeta;m,\mathsf{S})} \mathrm{d}y \int_{S(\zeta;y;m,\mathsf{S})} \mathrm{d}x \times I_h^{(n)}(\Delta_o, \Delta_h; \Phi|m; r_{\mathsf{S}}) \exp[-\mu_0(\Delta_o + \Delta_h)] \quad (42)$$

and expansion parameter:

$$\xi = |u| \times \zeta^2 = (t/2\Lambda_{oh} \cos\theta_{oh})^2. \quad (43)$$

As indicated in equation (42), the number of regions that should be included in the calculation of the expansion coefficients depends on the expansion order n. n should be greater or equal to $n_{\min}(m)$ before the region m contributes. The physical reason is that, for the wavefield to reach that particular region, it has to experience a certain number of scattering–rescattering events. It is found that

$$n_{\min}(m) = m/2 \qquad \textit{Bragg} \text{ family}$$
$$n_{\min}(m) = (m+3)/6 \qquad \textit{Laue} \text{ family},$$

where integer division is understood.

It now becomes straightforward to calculate the ordinary absorption factor A for the $t \times l$ crystal in the symmetrical scattering case. In the kinematical limit, *i.e.* when $n = 0$, we have no multiple scattering and

$$A = f_0^{(q)}(\zeta, \mu_0).$$

The regions $m = m_0'(\zeta; \mathsf{S})$ that will contribute have a zeroth-order term in their field expansion and for those regions

$$G_h^{(0)}(\Delta_o, \Delta_h|m_0'(\zeta; \mathsf{S}); r_{\mathsf{S}}) = 1. \quad (44)$$

We write:

$$A = A(\zeta, \mu_0) = (1/2\zeta) \sum_{\mathsf{S}} \sum_{m=m_0'(\zeta;\mathsf{S})} \int_{M(\zeta;m,\mathsf{S})} \mathrm{d}y \int_{S(\zeta;y;m,\mathsf{S})} \mathrm{d}x \times \exp[-\mu_0(\Delta_o + \Delta_h)]. \quad (45)$$

3. Results

3.1. *Series expansion – asymptotic properties*

By studying the contributions to the diffracted field originating from different regions within the crystal, we find that an asymptotic value of the series-expansion coefficients is reached, when the pure Laue (*B–D*) contribution equals zero. In terms of scattering–rescattering events, each region in the two families can be characterized by a minimum number of events necessary to reach the region. Since the expansion order n corresponds to the number of such events, we have that the asymptotic level occurs when an increase of ζ (or equivalently q) gives no additional field contributions to that particular order, *cf.* §2.6. The asymptotic expression depends only upon the *A–A*, *B–A* and *A–D* scattering processes. This type of field regime should occur when

$$q \to q_n = 2(n/2) + 2, \quad (46)$$

where $n/2$ denotes integer division.

Thus, for $q \geq q_n$:

$$f_n^{(q)} = f_n^{(\mathrm{Asymp})}.$$

Such a pattern is observed when normal absorption is included, *cf.* §3.3. In the case of zero absorption, the asymptotic behaviour occurs already when

$$q_n = n. \tag{47}$$

In this case, the contribution from the pure Laue field, *B–D*, is different from zero. However, contributions from *A–A*, *B–A* and *A–D* scattering effectively cancel it out, leaving the asymptotic expression.

We also find that the contribution from *B–A* scattering generally equals that from the *A–D* scattering. This may qualitatively be explained by simple symmetry arguments: When reversing the scattering process, the *B–A* case represents the *A–D* case and *vice versa*. Furthermore, the expansion coefficients $f_n^{(q)}$ do not depend on the parameter o, which merely labels two different integration schemes giving the same final result.

The kinematical limit is given by the zeroth-order expansion coefficient† f_0^q. Table 8 gives the analytical expressions for the various contributions to f_0 in the zero-absorption case. The different terms add to 1 for all ζ. Fig. 8 illustrates the functional dependence upon ζ. We notice that Laue transmission (*B–D* scattering) is dominant when $\zeta \leq 4/5$ while Bragg reflection (*A–A* scattering) gives the main contribution when $\zeta \geq 2$. In the range $4/5 \leq \zeta \leq 2$, the mixed scattering terms are the most important.

By using equation (42), we are able to analytically calculate the series-expansion coefficients, $f_n^{(q)}$. The results up to $n = 4$ are shown in Fig. 9. The curves are all continuous over every interval specified by q, and are descending functions of ζ. Using equation (41), we find for the primary extinction factors‡ for the first three ζ ranges:

$$y_p^{(q=0)} = 1 - (2/3)(2 - \zeta)\xi + (4/45)(9 - 5\zeta)\xi^2 - \ldots \tag{48}$$

$$y_p^{(q=1)} = 1 - (2/3\zeta^3)(-1 + 2\zeta)\xi + (4/45\zeta^5)(10 - 24\zeta + 40\zeta^3 - 30\zeta^4 + 9\zeta^5 - \zeta^6)\xi^2 - \ldots \tag{49}$$

$$y_p^{(q=2)} = 1 - (2/3\zeta^3)(-1 + 2\zeta)\xi + (8/45\zeta^5)(-11 + 12\zeta)\xi^2 - \ldots. \tag{50}$$

The series-expansion results have been used to verify and extend the extinction factor curves given by Olekhnovich & Olekhnovich (1978) for the special case of a square-cross-section crystal (Larsen, 1997). Within their domain of applicability, the agreement with the present treatment seems to be exact.

† When it is not explicitly necessary, we do not use the (q) label for the coefficients $f_n^{(q)}$.

‡ We reserve the symbol y_p for the case when only multiple scattering is included in the calculation. For convenience, only results up to second order are shown.

Table 8. *Expansion coefficients f_0 for the various scattering processes*

Scattering	$\zeta \leq 1$	$1 \leq \zeta \leq 2$	$\zeta \geq 2$
A–A	$\zeta/4$	$\zeta/4$	$1-1/\zeta$
A–D = *B–A*	$\zeta/4$	$1-1/2\zeta-\zeta/4$	$1/2\zeta$
B–D	$1-3\zeta/4$	$-1+1/\zeta+\zeta/4$	0

Now consider only the Laue contribution (*B–D*) for $q = 0$. This is found to be

$$y_p^{(B-D)} = [1 - (3/4)\zeta] - [4/3 - (23/24)\zeta]\xi + [4/5 - (379/720)\zeta]\xi^2 - [16/63 - (99/640)\zeta]\xi^3 + \ldots. \tag{51}$$

In the case of a semi-infinite crystal plate, $l \to \infty$ and hence $\zeta \to 0$. Applying this condition to equation (51) and introducing a modified expansion parameter, ξ_L, by $\xi = \frac{1}{4}\xi_L$ or

$$\xi_L = (t/\Lambda_{oh} \cos\theta_{oh})^2, \tag{52}$$

we get the following series solution for the primary

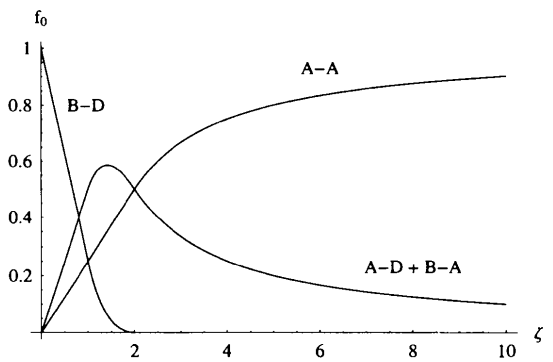

Fig. 8. Contributions to the kinematical integrated power from the various scattering processes.

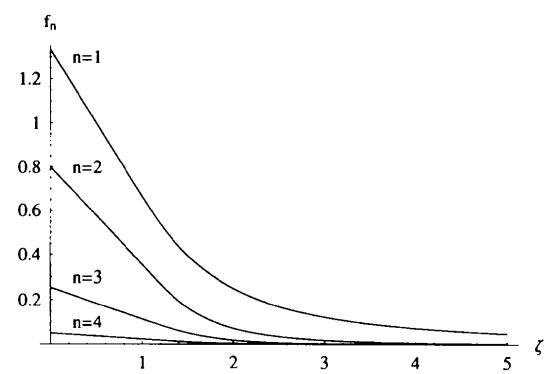

Fig. 9. Series-expansion coefficients, $f_n^{(q)}$, as a function of ζ for $n = \{1, 2, 3, 4\}$. $\mu = 0$ and $\Phi = 0$.

(Laue) extinction factor:

$$y_p = 1 - (1/3)\xi_L + (1/20)\xi_L^2 - (1/252)\xi_L^3 + \ldots$$
$$= (1/\xi_L^{1/2}) \sum_n J_{2n+1}(2\xi_L^{1/2}). \quad (53)$$

This result is identical to the well known expression for Laue transmission in a perfect semi-infinite crystal plate first derived by Zachariasen (1945, 1967).

The pure Bragg contribution (A–A) to the extinction factor in the asymptotic limit is:

$$y_p^{(\text{Asymp},A-A)} = (-1+\zeta)/\zeta - [2(-3+2\zeta)/3\zeta^3]\xi + [8(-23+12\zeta)/45\zeta^5]\xi^2 - [32(-79+34\zeta)/315\zeta^7]\xi^3 + \ldots. \quad (54)$$

Redefining the expansion coefficient,

$$\xi_B = 4\xi/\zeta^2 = (l/\Lambda_{oh}\sin\theta_{oh})^2, \quad (55)$$

and using it in the appropriate limit, $\zeta \to \infty$, we get the following series solution for the primary extinction factor:

$$y_p = 1 - (1/3)\xi_B + (2/15)\xi_B^2 - (17/315)\xi_B^3 + \ldots$$
$$= (\tanh \xi_B^{1/2})/\xi_B^{1/2}, \quad (56)$$

which is the familiar expression for a symmetrical Bragg reflection in a semi-infinite crystal (Darwin, 1922; Zachariasen, 1945).

The expansion for the primary extinction factor, equation (41), is a slowly convergent series. This is illustrated in Fig. 10 where the upper limit in ξ, corresponding to an upper bound in the absolute error in the calculated extinction factor of 10^{-4}, is shown as a function of ζ. A series expansion including the tenth-order term is used in this calculation. Although both ξ and ζ are functions of t, l and θ_{oh}, which renders some degrees of freedom, it is clear that numerical methods are necessary to increase the potential of our approach.

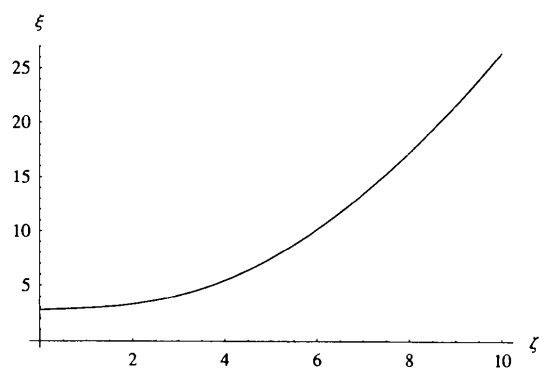

Fig. 10. Limiting value of the expansion parameter ξ as a function of the parameter ζ. Actual values of ξ should stay below the limiting curve to keep the absolute error in the calculation of the extinction factor within 10^{-4}. Ten terms are used in the series expansion.

3.2. *Numerical results for the primary extinction factor*

By using equation (13) together with Uragami's results for the boundary-value Green functions, *cf.* §2.4.2, we are able to perform numerical integrations giving the primary extinction factor for a range of different scattering conditions. In Figs. 11, 12 and 13, y_p is plotted as a function of t/Λ_{oh} for $\theta_{oh} \in (5°, 30°, 55°)$ with $t/l = 1/4$ and 4. The case of $\theta_{oh} = 5°$, $t/l = 1/4$ is very close to the 'pure' Laue situation. On the other

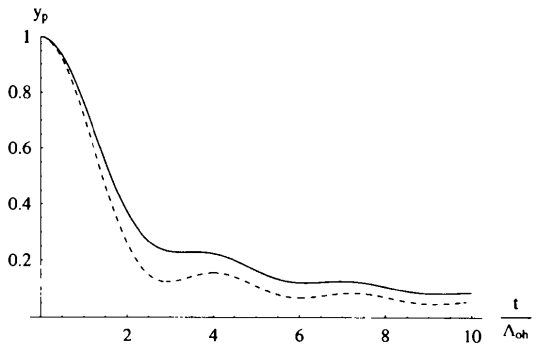

Fig. 11. Primary extinction factor for $\theta_{oh} = 5°$ as a function of t/Λ_{oh}. Solid line: $t/l = 4$, dashed line: $t/l = 1/4$.

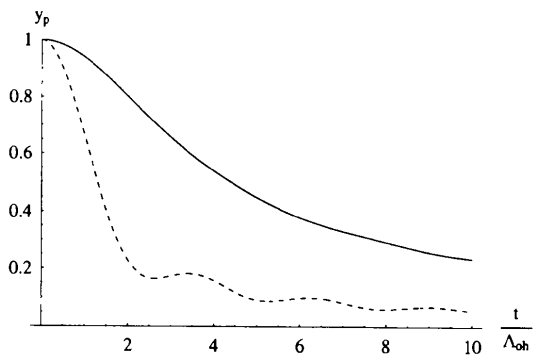

Fig. 12. Primary extinction factor for $\theta_{oh} = 30°$ as a function of t/Λ_{oh}. Solid line: $t/l = 4$, dashed line: $t/l = 1/4$.

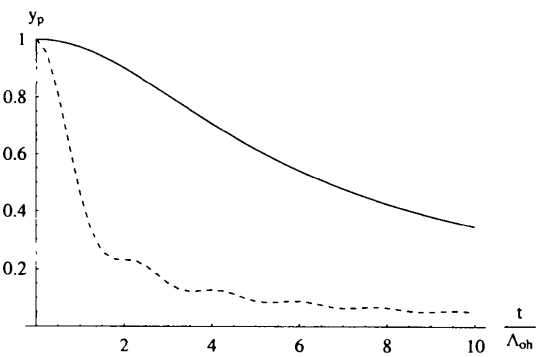

Fig. 13. Primary extinction factor for $\theta_{oh} = 55°$ as a function of t/Λ_{oh}. Solid line: $t/l = 4$, dashed line: $t/l = 1/4$.

hand, the case of $\theta_{oh} = 55°$, $t/l = 4$ is close to the 'pure' Bragg situation, as is shown in Fig. 14. When $\zeta \leq 0.02$, the function (53) approximates the true extinction factor with an error $\lesssim 5\%$, while for $\zeta \geq 6$ the function (56) gives results $\lesssim 8\%$ from the true values.

3.3. *Absorption*

By taking photoelectric absorption into account through the dimensionless parameter μ_0 defined in equation (14), we find expressions for the normal absorption factor A using equation (45). We obtain: for $q = 0$ $(0 \leq \zeta \leq 1)$:

$$A = [-1 + \exp(2\mu_0\zeta) - 4\mu_0\zeta + 2\mu_0\zeta\exp(2\mu_0\zeta) + 8\mu_0^2\zeta - 6\mu_0^2\zeta^2]/8\mu_0^2\zeta\exp(2\mu_0\zeta); \quad (57)$$

for $q = 1$ $(1 \leq \zeta \leq 2)$:

$$A = 1/\zeta\exp(2\mu_0\zeta) + 1/8\mu_0^2\zeta - 1/2\mu_0^2\zeta\exp(2\mu_0) + 3/8\mu_0^2\zeta\exp(2\mu_0\zeta) - 1/\mu_0\zeta\exp(2\mu_0\zeta) - 1/\exp(2\mu_0\zeta) + 1/4\mu_0 + 1/2\mu_0\exp(2\mu_0\zeta) + \zeta/4\exp(2\mu_0\zeta). \quad (58)$$

The asymptotic regime for $n = 0$ occurs, according to equation (46), when $q = 2$. Thus, equation (59) covers the whole range $\zeta \geq 2$.

$$A = [3 - 4\exp(2\mu_0) + \exp(4\mu_0) + 4\mu_0 - 2\mu_0\zeta + 2\mu_0\zeta\exp(4\mu_0)]/8\mu_0^2\zeta\exp(4\mu_0). \quad (59)$$

Considering a semi-infinite crystal, we obtain expressions identical to those found in the literature (Maslen, 1995). Fig. 15 shows the absorption factor as a function of ζ with μ_0 as parameter.

The results given by equations (57)–(59) might serve as checkpoints for the algorithms used for absorption correction in crystallographic computing, *cf.* Hall *et al.* (1995).

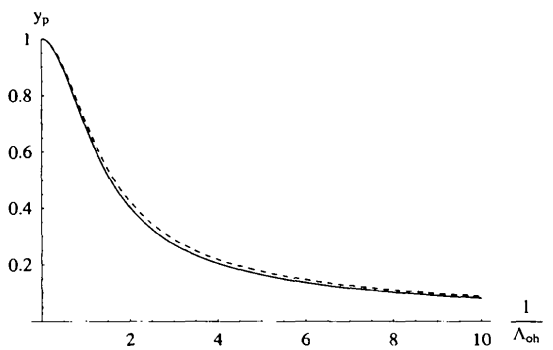

Fig. 14. Comparison of the calculated primary extinction factor for $\theta_{oh} = 55°$ and $t/l = 4$ (dashed line) with the Bragg curve (solid line) from the fundamental theory, both as functions of l/Λ_{oh}.

3.4. *Generalized extinction factor*

The combined attenuation effect from both normal absorption and multiple scattering is taken into account when calculating the generalized extinction factor y. In Fig. 16, we have compared the generalized extinction factor y with $y_p \times A$. It is seen that for the transmission case, $\theta_{oh} = 0°$, the curves overlap. This is because all

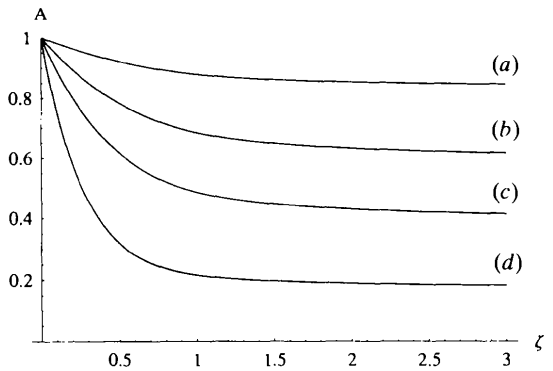

Fig. 15. Absorption factor as a function of ζ. (*a*) $\mu_0 = 0.1$, (*b*) $\mu_0 = 0.3$, (*c*) $\mu_0 = 0.6$ and (*d*) $\mu_0 = 1.5$.

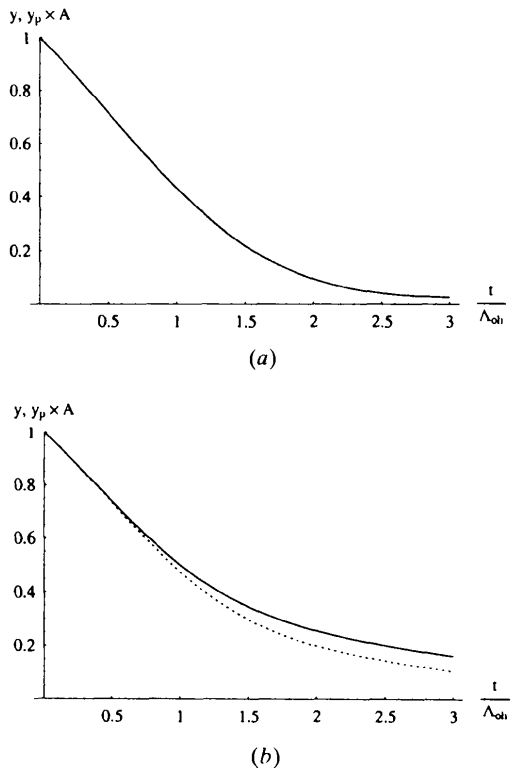

Fig. 16. Comparison between the generalized extinction factor, y, (solid line) and the product $y_p \times A$ (dashed line) for a square-cross-section ($t/l = 1$) crystal. Case (*a*) is calculated for $\theta_{oh} = 0°$ and case (*b*) for $\theta_{oh} = 45°$. The absorption factor is chosen such that $\mu\Lambda_{oh} = 0.5$.

scattering routes will have the same effective path length. For $\theta_{oh} > 0°$, this is not the case. Here the contributions do not factorize and $y > y_p \times A$ for every t/Λ_{oh}.

In structural analysis, the factorization scheme is adopted in the data reduction but one tries to bypass the above problem by using absorption-weighted mean free path lengths in a refinement of the extinction factor, *cf.* Becker & Coppens (1974*a*,*b*, 1975).

Anomalous scattering may also be included in the generalized extinction factor through the phase angle Φ, equation (7), and by using amplitude-corrected structure factors (knowing f' and f'') in the calculation of the extinction length, Λ_{oh}, equation (8). In a model study on small germanium crystals, we have used the present formalism combined with the anomalous scattering factors calculated by Kissel and co-workers (Kissel *et al.*, 1995) to investigate the generalized extinction factor as a function of the wavelength of the incident radiation. An example for the moderately strong $\bar{1}\bar{3}1$ reflection is shown in Fig. 17. $\Phi_{\bar{1}\bar{3}1}(\lambda)$ and $\Lambda_{\bar{1}\bar{3}1}(\lambda)$ are given in Figs. 18 and 19. The prominent feature of the set of curves in Fig. 17 is the photoelectric K threshold apparent at $\lambda \simeq 1.1211$ Å. We observe that the extinction factors approach unity (*i.e.* the kinematical limit) when $\lambda \to 0$. As the wavelength increases, the extinction curves decrease smoothly towards the photoelectric threshold. A more rapid decrease is observed as the crystal dimension increases. At the threshold, resonant scattering is of great importance. However, the theory for calculating f' and f'' is not capable of adequately describing resonance effects that take place here, leading to unreliable values in the correction terms (Kissel *et al.*, 1995; Cromer & Liberman, 1970).

Finally, at the low-energy side of the threshold, the attenuation is of course reduced owing to the reduction of the photoelectric absorption coefficient, but the extinction factor curves continue to decrease as the wavelength increases. It is however interesting to note the different rates at which the curves decline. The effect of crystal dimension is important, and at the two highest values, $t = \{8, 10\}$ μm, the curves tend to flatten out. It has been found (Larsen, 1997) that for stronger reflections the generalized extinction factors show an oscillating behaviour as a function of λ for low energies.

4. Conclusions

The boundary-value Green function technique combined with the Takagi–Taupin equations comprises a powerful tool in handling dynamical X-ray scattering in finite crystals. We have shown how to obtain generalized extinction factors for a rectangular $t \times l$ crystal geometry. The analytical calculations confirm the findings from standard plane-wave fundamental theory in the limit of a semi-infinite crystal plate. A key to the success of the method is its easy implementation in a symbolic software system such as *Mathematica*. This enables us to perform series expansions in principle to

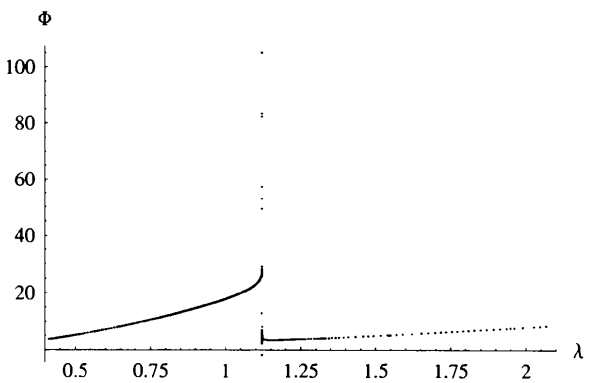

Fig. 18. The phase sum Φ (°) as a function of the wavelength λ (Å) for the $\bar{1}\bar{3}1$ reflection in germanium.

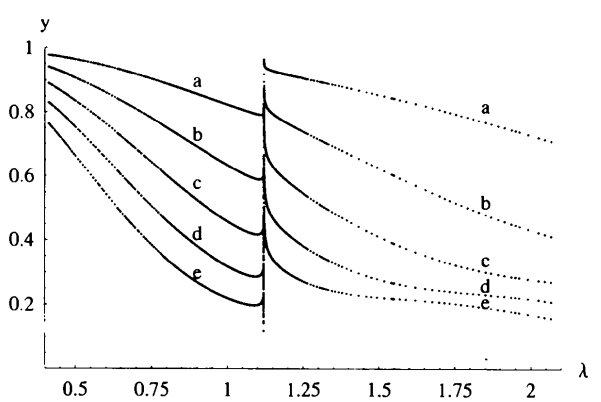

Fig. 17. Generalized extinction factor as a function of wavelength λ (Å) for crystal dimensions $\{a, b, c, d, e\} = \{2, 4, 6, 8, 10\}$ μm. Germanium, reflection $\bar{1}\bar{3}1$; square-cross-section crystal geometry ($t/l = 1$).

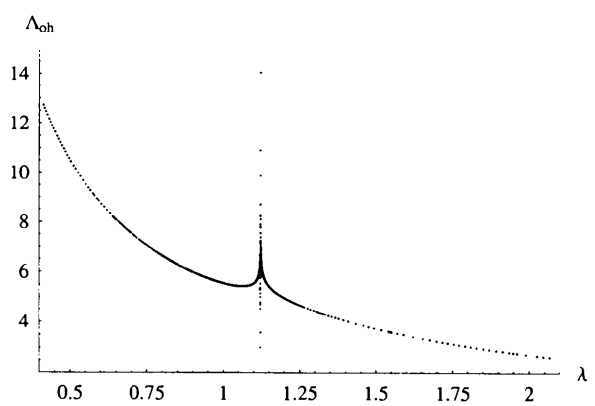

Fig. 19. The extinction length Λ_{oh} (μm) as a function of the wavelength λ (Å) for the $\bar{1}\bar{3}1$ reflection in germanium.

Table 9. *Coordinates for a point M on an exit surface in relation to a source point S*

Surfaces	Δ_o	Δ_h
A–A	$(1/2\cos\theta_{oh})[r_o(M) - r_o(S)]$	$(1/2\cos\theta_{oh})[r_o(M) - r_o(S)]$
A–D	$(1/2\cos\theta_{oh})[t - r_o(S)] + (1/2\sin\theta_{oh})r_1(M)$	$(1/2\cos\theta_{oh})[t - r_o(S)] - (1/2\sin\theta_{oh})r_1(M)$
B–A	$(1/2\cos\theta_{oh})r_o(M) - (1/2\sin\theta_{oh})r_1(S)$	$(1/2\cos\theta_{oh})r_o(M) + (1/2\sin\theta_{oh})r_1(S)$
B–D	$(1/2\cos\theta_{oh})t + (1/2\sin\theta_{oh})[r_1(M) - r_1(S)]$	$(1/2\cos\theta_{oh})t - (1/2\sin\theta_{oh})[r_1(M) - r_1(S)]$

Table 10. *Change of variables – definitions*

Surfaces	Entrance	Exit
A–A	$r_0(S) = r_0(M) - 2\cos\theta_{oh}x$	$r_0(M) = 2\cos\theta_{oh}y$
A–D	$r_0(S) = t - [r_1(M)/\tan\theta_{oh}] - 2\cos\theta_{oh}x$	$r_1(M) = 2\sin\theta_{oh}y$
B–A	$r_1(S) = 2\sin\theta_{oh}x - r_0(M)\tan\theta_{oh}$	$r_0(M) = 2\cos\theta_{oh}y$
B–D	$r_1(S) = 2\sin\theta_{oh}x + r_1(M) - t\tan\theta_{oh}$	$r_1(M) = 2\sin\theta_{oh}y$

any order. However, for higher-order terms, the calculations become very complex and time and memory consuming, and numerical methods become necessary.

The extension of this work to the case of non-symmetrical scattering, which increases the geometrical complexity of the problem, will be the subject of a forthcoming paper, *cf.* Thorkildsen & Larsen (1997).

APPENDIX *A*

A1. Coordinate systems

With the origin of the local coordinate system on the entrance surface A, the relation between the local (s_o, s_h) and global (r_0, r_1) coordinates for a general point within the crystal is given by

$$\begin{aligned} s_o &= (1/2\cos\theta_{oh})[r_0 - r_0(S)] + (1/2\sin\theta_{oh})r_1 \\ s_h &= (1/2\cos\theta_{oh})[r_0 - r_0(S)] - (1/2\sin\theta_{oh})r_1. \end{aligned} \tag{60}$$

With the origin of the local coordinate system on the entrance surface B, the relation between the local and global coordinates for a general point is given by

$$\begin{aligned} s_o &= (1/2\cos\theta_{oh})r_0 + (1/2\sin\theta_{oh})[r_1 - r_1(S)] \\ s_h &= (1/2\cos\theta_{oh})r_0 - (1/2\sin\theta_{oh})[r_1 - r_1(S)]. \end{aligned} \tag{61}$$

A2. Coordinates for an exit point M

It is convenient to represent an exit point M in the (r_0, r_1) coordinate system. On exit surface A, $r_0(M) \in (0, t)$ and $r_1(M) = 0$, while, on exit surface D, $r_0(M) = t$ and $r_1(M) \in (0, l)$. The coordinates for an exit point with respect to the appropriate source point, *i.e.* Δ_o and Δ_h, are given in Table 9.

A3. Definition of new variables

The surface integrations are simplified by introducing a set of variables, (x, y), with somewhat different definitions according to the actual combination of entrance and exit surfaces. The definitions are given in Table 10.

References

Azároff, L. V., Kaplow, R., Kato, N., Weiss, R., Wilson, A. & Young, R. (1974). *X-ray Diffraction.* New York: McGraw-Hill.

Becker, P. (1977). *Acta Cryst.* A**33**, 667–671.

Becker, P. & Coppens, P. (1974*a*). *Acta Cryst.* A**30**, 129–147.

Becker, P. & Coppens, P. (1974*b*). *Acta Cryst.* A**30**, 148–153.

Becker, P. & Coppens, P. (1975). *Acta Cryst.* A**31**, 417–425.

Becker, P. & Dunstetter, F. (1984). *Acta Cryst.* A**40**, 241–251.

Cromer, D. & Liberman, D. (1970). *J. Chem. Phys.* **53**, 1891–1898.

Darwin, C. G. (1922). *Philos. Mag.* **43**, 800–829.

Hall, S. R., King, G. S. D. & Stewart, J. M. (1995). *Xtal3.4 User's Manual.* Lamb, Perth: University of Western Australia.

Kissel, L., Zhou, B., Roy, S. C., SenGupta, S. K. & Pratt, R. H. (1995). *Acta Cryst.* A**51**, 271–288.

Larsen, H. B. (1997). Doctoral thesis, The Norwegian University of Science and Technology, Trondheim, Norway.

Maslen, E. N. (1995). *International Tables for Crystallography*, Vol. C, edited by A. J. C. Wilson, pp. 520–529. Dordrecht: Kluwer Academic Publishers.

Olekhnovich, N. M. & Olekhnovich, A. I. (1978). *Acta Cryst.* A**34**, 321–326.

Pinsker, Z. G. (1978). *Dynamical Scattering of X-rays in Crystals.* Berlin: Springer-Verlag.

Saka, T., Katagawa, T. & Kato, N. (1972*a*). *Acta Cryst.* A**28**, 102–113.

Saka, T., Katagawa, T. & Kato, N. (1972*b*). *Acta Cryst.* A**28**, 113–120.

Saka, T., Katagawa, T. & Kato, N. (1973). *Acta Cryst.* A**29**, 192–200.

Sneddon, I. N. (1957). *Elements of Partial Differential Equations.* London: McGraw-Hill.

Snigirev, A. A. & Suvorov, A. Y. (1993). *Acta Cryst.* A**49**, 818–824.

Sommerfeld, A. (1949). *Partial Differential Equations.* New York: Academic Press.

Takagi, S. (1962). *Acta Cryst.* **15**, 1311–1312.

Takagi, S. (1969). *J. Phys. Soc. Jpn*, **26**, 1239–1253.

Taupin, D. (1964). *Bull. Soc. Fr. Minéral. Cristallogr.* **87**, 469–511.

Thorkildsen, G. & Larsen, H. B. (1997). *Two Beam Diffraction in Perfect Crystals Analyzed by Takagi's Equations.* Part 1. *Basic Principles and Methods of Solution.* Technical Report 30. Stavanger College, Stavanger, Norway.

Thorkildsen, G. & Larsen, H. B. (1998). *Acta Cryst.* A**54**, 172–185.
Uragami, T. S. (1969). *J. Phys. Soc. Jpn*, **27**, 147–154.
Uragami, T. S. (1970). *J. Phys. Soc. Jpn*, **28**, 1508–1527.
Uragami, T. S. (1971). *J. Phys. Soc. Jpn*, **31**, 1141–1161.
Zachariasen, W. H. (1945). *Theory of X-ray Diffraction in Crystals*. London: John Wiley.
Zachariasen, W. H. (1967). *Acta Cryst.* **23**, 558–564.